arXiv:1606.08563v2 [cond-mat.supr-con] 19 Oct 2016

Nonsymmorphic Weyl superconductivity in UPt_3 based on E_{2u} representation

Youichi Yanase[1,*]

[1] *Department of Physics, Graduate School of Science, Kyoto University, Kyoto 606-8502, Japan*

(Dated: October 20, 2016)

We show that a heavy fermion superconductor UPt_3 is a topological Weyl superconductor with tunable Weyl nodes. Adopting a generic order parameter in the E_{2u} representation allowed by nonsymmorphic crystal symmetry, we clarify unusual gap structure and associated topological properties. The pair creation, pair annihilation, and coalescence of Weyl nodes are demonstrated in the time-reversal symmetry broken B-phase. At most 98 point nodes compatible with Blount's theorem give rise to line node-like behaviors in low-energy excitations, consistent with experimental results. We also show an *arc* node protected by the nonsymmorphic crystal symmetry on the Brillouin zone face.

Superconductivity with nontrivial symmetry and topology is attracting renewed interest stimulated by enormous studies of topological insulators and superconductors[1–4]. Strongly correlated electron systems are platform of such unconventional superconductivity[5]. A heavy fermion superconductor UPt_3 discovered in 1980's[6] unambiguously exhibits exotic properties, that is, multiple superconducting phases in the field-temperature plane [Fig. 1(a)][7–9]. The presence of the multiple superconducting phases is a direct evidence for a multicomponent non-s-wave order parameter[10]. Comparison between experiments and theories points to odd-parity spin-triplet superconductivity[11–13]. Because odd-parity superconductivity is often accompanied by topological order[2,14–16], it may be interesting to clarify the topological properties of UPt_3.

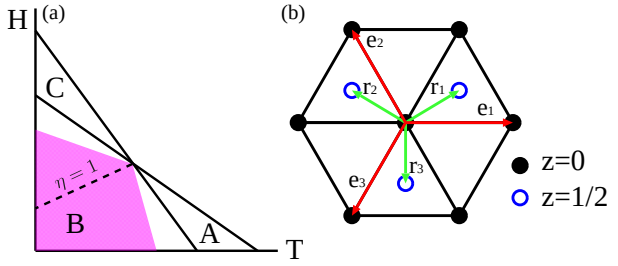

FIG. 1. (Color online) (a) Multiple superconducting phases in UPt_3. Shaded region shows the Weyl superconducting phase. (b) Crystal structure of UPt_3. Uranium ions form AB-stacked triangular lattice. Two-dimensional vectors, $\boldsymbol{e}_i$ and $\boldsymbol{r}_i$, are shown by arrows.

Topological order in superconductors is closely related to the symmetry and nodal structure of superconductivity. Despite intensive studies for three decades, the symmetry of superconductivity in UPt_3 is still under debate. However, a chiral f-wave state with orbital angular momentum $L_z = \pm 2$[11] allowed in hexagonal crystals [see Fig. 1(b)] is supported by nodal excitations[12] and broken time-reversal symmetry[17] as well as by a phase sensitive measurement[18]. On the other hand, a recent thermal conductivity measurement points to another f-wave state with $L_z = \pm 1$[19].

In spite of these intensive studies, the f-wave pairing states are incompatible with the Blount's theorem[20,21] which proves the absence of line node in odd-parity superconductors[22]. Although line node behaviors have been observed in UPt_3[12], Blount's theorem implies that line nodes are fragile against perturbation preserving the symmetry of the system. Indeed, the line nodes disappear as a result of the mixing of f-wave Cooper pairs with p-wave ones in the same irreducible representation. According to the symmetry classification[10], not only the chiral f-wave state with $L_z = \pm 2$[11] but also a p-wave state (and the f-wave state with $L_z = \pm 1$[19]) belong to the E_{2u} representation of D_{6h} point group. Therefore a generic E_{2u} state is induced by a mixed p+f-wave Cooper paring. In this paper we clarify the nodal gap structure and specify the topological properties of a generic E_{2u}-state in UPt_3. It is revealed that the B-phase is a Weyl superconducting state[24] analogous to Weyl semimetals[25–27] discovered recently[28–31]. We furthermore demonstrate pair creation, pair annihilation, and coalescence of Weyl nodes which do not occur in other chiral Weyl superconductors[32–35].

Our study is based on a Bogoliubov-de Gennes (BdG) Hamiltonian,

$$\begin{aligned}\mathcal{H}_{\rm BdG} = &\sum_{\boldsymbol{k},m,s} \xi(\boldsymbol{k}) c^\dagger_{\boldsymbol{k}ms} c_{\boldsymbol{k}ms} + \sum_{\boldsymbol{k},s} \Big[a(\boldsymbol{k}) c^\dagger_{\boldsymbol{k}1s} c_{\boldsymbol{k}2s} + \text{h.c.} \Big] \\ &+ \sum_{\boldsymbol{k},m,s,s'} \alpha_m \boldsymbol{g}(\boldsymbol{k}) \cdot \boldsymbol{s}_{ss'} c^\dagger_{\boldsymbol{k}ms} c_{\boldsymbol{k}ms'} \\ &+ \frac{1}{2} \sum_{\boldsymbol{k},m,m',s,s'} \Big[\Delta_{mm'ss'}(\boldsymbol{k}) c^\dagger_{\boldsymbol{k}ms} c^\dagger_{-\boldsymbol{k}m's'} + \text{h.c.} \Big], \quad (1)\end{aligned}$$

where $\boldsymbol{k}$, $m = 1, 2$, and $s = \uparrow, \downarrow$ are momentum, sublattice, and spin, respectively. Based on the crystal structure of UPt_3 illustrated in Fig. 1(b), we adopt an intra-sublattice kinetic energy, $\xi(\boldsymbol{k}) = 2t \sum_{i=1,2,3} \cos \boldsymbol{k}_\parallel \cdot \boldsymbol{e}_i + 2t_z \cos k_z - \mu$, and inter-sublattice hopping term, $a(\boldsymbol{k}) = 2t' \cos \frac{k_z}{2} \sum_{i=1,2,3} e^{i\boldsymbol{k}_\parallel \cdot \boldsymbol{r}_i}$, with $\boldsymbol{k}_\parallel = (k_x, k_y)$ and $\boldsymbol{e}_1 = (1, 0)$, $\boldsymbol{e}_2 = (-\frac{1}{2}, \frac{\sqrt{3}}{2})$, $\boldsymbol{e}_3 = (-\frac{1}{2}, -\frac{\sqrt{3}}{2})$, $\boldsymbol{r}_1 = (\frac{1}{2}, \frac{1}{2\sqrt{3}})$, $\boldsymbol{r}_2 = (-\frac{1}{2}, \frac{1}{2\sqrt{3}})$, and $\boldsymbol{r}_3 = (0, -\frac{1}{\sqrt{3}})$. Since D_{3h} local symmetry at Uranium ions lacks inversion symmetry, Kane-Mele spin-orbit coupling (SOC) with $\boldsymbol{g}(\boldsymbol{k}) =$

$\hat{z}\sum_{i=1,2,3}\sin \boldsymbol{k}_{\parallel}\cdot \boldsymbol{e}_i$[36] appears in a sublattice-dependent way. The coupling constant is $(\alpha_1,\alpha_2)=(\alpha,-\alpha)$ so as to preserve the global D_{6h} symmetry[1,37,38]. The inter-sublattice SOC is prohibited because the inter-sublattice bonds respect the inversion symmetry.

Quantum oscillation measurements combined with band structure calculations[12,39–42] have shown a pair of FSs centered at the A-point (A-FSs), three FSs at the Γ point (Γ-FSs), and two FSs at the K point in UPt_3. Since small FSs enclosing the K point give a small density-of-states (DOS), they may play a minor role. Therefore, we study the superconducting properties of A-FSs and Γ-FSs one by one. By choosing a parameter set $(t,t_z,t',\alpha,\mu)=(1,-4,1,2,12)$ our two band model reproduces a pair of A-FSs, while another set $(t,t_z,t',\alpha,\mu)=(1,4,1,0,16)$ reproduces topology of Γ-FS. Since the SOC is negligible for the Γ-FS, we simply set $\alpha=0$ in the latter parameter set.

Order parameter of the E_{2u}-state is generally represented by $\hat{\Delta}(\boldsymbol{k})=\eta_1\hat{\Gamma}_1+\eta_2\hat{\Gamma}_2$ with basis functions $\hat{\Gamma}_1$ and $\hat{\Gamma}_2$ composed of several components. Although the purely f-wave state has been intensively investigated[11], an admixture of a p-wave component is allowed by symmetry. Besides these components, a sublattice-singlet spin-triplet d-wave component naturally accompanies the f-wave component because of the nonsymmorphic crystal structure of UPt_3[43]. Taking into account all the components, we study the E_{2u}-state with

$$\hat{\Gamma}_1=\big[\delta\left\{p_x(\boldsymbol{k})s_x-p_y(\boldsymbol{k})s_y\right\}\sigma_0 +f_{(x^2-y^2)z}(\boldsymbol{k})s_z\sigma_x-d_{yz}(\boldsymbol{k})s_z\sigma_y\big]is_y, \quad (2)$$

$$\hat{\Gamma}_2=\big[\delta\left\{p_y(\boldsymbol{k})s_x+p_x(\boldsymbol{k})s_y\right\}\sigma_0 +f_{xyz}(\boldsymbol{k})s_z\sigma_x-d_{xz}(\boldsymbol{k})s_z\sigma_y\big]is_y, \quad (3)$$

where s_α and σ_α are Pauli matrix in the spin and sublattice space, respectively. The orbital functions, $p_i(\boldsymbol{k})$, $d_i(\boldsymbol{k})$, and $f_i(\boldsymbol{k})$, are obtained by assuming short-range Cooper pairs on neighboring $\boldsymbol{r}_i$ and $\boldsymbol{e}_i$ bonds[43]. This choice is consistent with empirical rules obtained by microscopic calculations for many unconventional superconductors[5]. We choose $|\delta|\ll 1$ to study a dominantly f-wave state. Two-component order parameters are parametrized as $(\eta_1,\eta_2)=\Delta(1,i\eta)/\sqrt{1+\eta^2}$ by a real parameter η. Ratio of η_1 and η_2 is pure-imaginary since the condensation energy is maximally gained in the chiral superconducting state. Thus, the B-phase is a chiral state where the range of η is $0<\eta<\infty$[44]. It is believed that a weak breakdown of hexagonal symmetry stabilizes the A- and C-phases[11,12,44–46]. We assume that the A-phase is the Γ_2-state ($\eta=\infty$), while the C-phase is the Γ_1-state ($\eta=0$).

The BdG Hamiltonian is represented in the Nambu space $\mathcal{H}_{\rm BdG}=\frac{1}{2}\sum_{\boldsymbol{k}}\hat{c}^\dagger_{\boldsymbol{k}}\hat{H}_{\rm BdG}(\boldsymbol{k})\hat{c}_{\boldsymbol{k}}$, with $\hat{c}_{\boldsymbol{k}}=(c_{\boldsymbol{k}1\uparrow},c_{\boldsymbol{k}2\uparrow},c_{\boldsymbol{k}1\downarrow},c_{\boldsymbol{k}2\downarrow})^{\rm T}$. In order to study topological properties, we perform a unitary transformation $\tilde{H}_{\rm BdG}(\boldsymbol{k})=U(\boldsymbol{k})\hat{H}_{\rm BdG}(\boldsymbol{k})U(\boldsymbol{k})^\dagger$. By choosing $U(\boldsymbol{k})=\begin{pmatrix}1&0\\0&e^{i\boldsymbol{k}\cdot\boldsymbol{\tau}}\end{pmatrix}_\sigma\otimes s_0\otimes\tau_0$ and $\boldsymbol{\tau}=(0,-\frac{1}{\sqrt{3}},\frac{1}{2})$, $\tilde{H}_{\rm BdG}(\boldsymbol{k})$ is periodic with respect to the translation $\boldsymbol{k}\to\boldsymbol{k}+\boldsymbol{K}$ with $\boldsymbol{K}$ being a reciprocal lattice vector.

Weyl nodes are specified by a topological Weyl charge defined by a monopole of Berry flux, $q_i=\frac{1}{2\pi}\oint_S \mathrm{d}\boldsymbol{k}\vec{F}(\boldsymbol{k})$, where the Berry flux

$$F_i(\boldsymbol{k})=-i\varepsilon^{ijk}\sum_{E_n(\boldsymbol{k})<0}\partial_{k_j}\langle u_n(\boldsymbol{k})|\partial_{k_k}u_n(\boldsymbol{k})\rangle, \quad (4)$$

is integrated on a closed surface surrounding an isolated point node. We identify Weyl nodes by calculating k_z-dependent Chern number,

$$\nu(k_z)=\frac{1}{2\pi}\int \mathrm{d}\boldsymbol{k}_{\parallel}F_z(\boldsymbol{k}), \quad (5)$$

on a two-dimensional k_x-k_y-plane[47–49]. A wave function and energy of Bogoliubov quasiparticles are denoted by $|u_n(\boldsymbol{k})\rangle$ and $E_n(\boldsymbol{k})$, respectively. A jump in the Chern number is equivalent to the sum of Weyl charges at k_z. That is, $\nu(k_z+0)-\nu(k_z-0)=\sum_i q_i$. Thus, counting symmetry-related point nodes and comparing it with a jump in $\nu(k_z)$, we are able to identify Weyl charges.

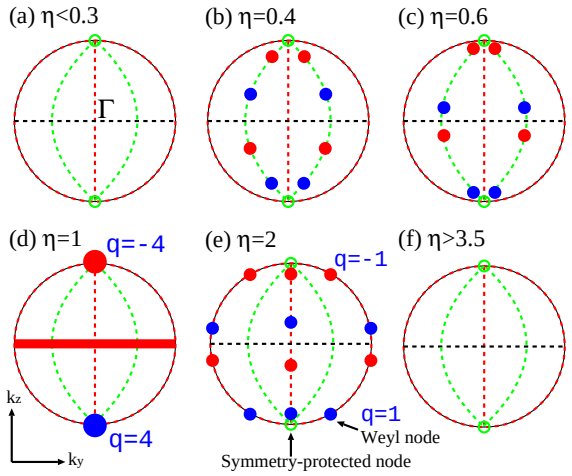

FIG. 2. (Color online) Illustration of pair creation and annihilation of Weyl nodes on a Γ-FS. Projection from the k_x-axis is shown. (b), (c) and (e), blue and red closed circles show single Weyl nodes with $q_i=1$ and -1, respectively. Large circles in (d) are spin-degenerate double Weyl nodes with $q_i=\pm4$. Thick solid line in (d) shows a quadratic line node at $k_z=0$. Green open circles are trivial point nodes protected by symmetry. Dashed lines illustrate nodal lines in the purely f-wave states, although they disappear in a generic E_{2u}-state.

First, we elucidate Weyl nodes on the Γ-FS. This is a simple case, because only one of the bands crosses the Fermi level although the two-band model is adopted. The nodal structures are qualitatively the same as those in the single-band model which are analytically expressed in appendix[50]. Then, the d-wave order parameter does not play any important role. On the other hand, the

p-f mixing in the order parameter eliminates line nodes in the chiral f-wave state[11] in accordance with Blount's theorem[20,21], except for $\eta = 1$, Diagonalizing $\tilde{H}_{\rm BdG}(\boldsymbol{k})$, we obtain the superconducting gap illustrated in Fig. 2. Instead of line nodes, Weyl nodes (closed circles in Fig. 2) appear in the B-phase, in addition to the symmetry-protected point nodes at the poles on the FS. The former is identified as Weyl nodes by Fig. 3(a). The Chern number jumps by ± 4, and we find four point nodes at a certain k_z. Thus, the point nodes are identified as single Weyl nodes with a unit charge $q_i = \pm 1$. In total, eight pairs of single Weyl nodes are produced. Since the spin degeneracy is lifted owing to the non-unitary order parameter, the spinless single Weyl nodes are realized even at zero magnetic field.

Here we show pair creation, annihilation and coalescence of Weyl nodes. Because the particle-hole symmetry is implemented in the BdG Hamiltonian for superconductors, the time-reversal symmetry ensures the chiral symmetry prohibiting Weyl nodes[51]. Therefore, the A- and C-phases do not host Weyl nodes as illustrated in Figs. 2(a) and (f). The triviality is robust against a weak time-reversal-symmetry-breaking because the gap-closing is required for the topological transition. Therefore, pair creation of Weyl nodes does not occur at the thermodynamical A-B and B-C phase boundaries, but occurs in the B-phase. For the parameters in Fig. 3(a), we see the pair creation at $\eta = 0.3$ and 3.5. Accordingly, the Weyl superconducting phase is illustrated in Fig. 1(a).

When the parameter η is increased from zero by decreasing the magnetic field or increasing the temperature, the Weyl nodes emerge and move along nodal lines of the $f_{(x^2-y^2)z}$-wave component [Figs. 2(b) and (c)]. At $\eta = 1$, four pairs of Weyl nodes cause pair annihilation at $k_z = 0$, and remaining eight Weyl nodes coalesce into a pair of spin-degenerate double Weyl nodes ($q_i = \pm 4$) at the poles [Fig. 2(d)]. When η increases from unity, eight pairs of Weyl nodes again appear on nodal lines of the f_{xyz}-wave component [Fig. 2(e)]. These pair creation, pair annihilation, and coalescence of Weyl nodes occur in the generic E_{2u}-state as a result of the p-f mixing[50], although the chiral f-wave state hosts only Weyl nodes at the poles which are shown in Fig. 2(d)[35].

The pair annihilation and coalescence of Weyl nodes give rise to unusual gap structure at $\eta = 1$. Since the B-phase is weakly non-unitary due to small δ, two non-equivalent superconducting gaps $\Delta_{\pm}(\boldsymbol{k})$ are obtained[10]. We see an intriguing nodal structure in the small gap $\Delta_{-}(\boldsymbol{k})$. The pair annihilation leads to *quadratic line node* at $k_z = 0$, that is, $\Delta_{-}(\boldsymbol{k}) \propto |k_z|^2$, which is distinct from a usual linear line node with $\Delta(\boldsymbol{k}) \propto |k_z|$ and gives rise to a low-energy DOS, $\rho(\omega) \propto \sqrt{\omega}$. On the other hand, the coalescence of Weyl nodes results in *cubic point nodes*, $\Delta_{-}(\boldsymbol{k}) \propto |\boldsymbol{k}_{\parallel}|^3$, at the poles.

Next, we investigate the A-FSs. This is an intriguing case, because the nonsymmorphic crystal symmetry causes gap nodes. The inter-sublattice hybridyzation

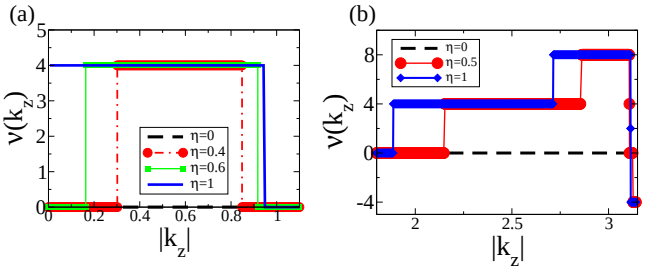

FIG. 3. (Color online) Chern number of the two-dimensional BdG Hamiltonian parametrized by k_z for (a) a Γ-FS reproduced by the parameter set $(t, t_z, t', \alpha, \mu, \Delta, \delta) = (1, 4, 1, 0, 16.0.4, 0.01)$ and for (b) A-FSs by $(1, -4, 1, 0, 12, 0.1, 0.04)$.

$a(\boldsymbol{k})$ vanishes at $k_z = \pi$, and resulting sublattice degeneracy leads to paired FSs, as shown in Fig. 5(a). Although the degeneracy is partly lifted by the SOC, the symmetry protects the degeneracy along $\boldsymbol{k}_{\parallel} \parallel [010]$ and symmetric lines (A-L lines)[52]. Thus, any single band model breaks down, and our two-band model is a minimal model.

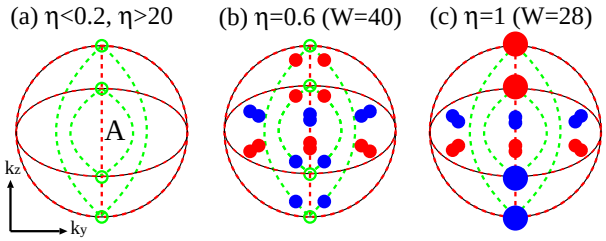

FIG. 4. (Color online) Illustration of Weyl nodes on the A-FSs drawn by numerically diagonalizing the BdG Hamiltonian for the parameter set in Fig. 3(b). Thin solid lines show paired FSs. Other marks are the same as Fig. 2. We show the number of Weyl nodes W.

Figure 3(b) shows an increase in the Chern number $\nu(k_z) = 0 \to 4 \to 8$ with $|k_z|$, indicating eight pairs of single Weyl nodes. These Weyl nodes arise from the p-f-mixing as we clarified for the Γ-FS. The Chern number $\nu(k_z) = 8$ is obtained just by the multiplication 2 due to the two-bands. When we furthermore increase $|k_z|$ to π, interestingly the Chern number changes to -4 given by the d-wave component of the order parameter. Since the sublattice-singlet d-wave component induces inter-band pairing, it is negligible in most region of the Brillouin zone. However, the inter-band pairing may play an important role around $k_z = \pi$ where the two bands are nearly degenerate. The jump of Chern number, $\nu(k_z) = 8 \to -4$, results in twelve pairs of single Weyl nodes. Twenty pairs of Weyl nodes appear on the A-FSs in total [Fig. 4(b)]. In contrast to eight pairs due to the p-f-mixing, the twelve pairs of Weyl nodes arising from the d-f-mixing in the order parameter are robust in the six-fold rotation-symmetric state at $\eta = 1$ [Fig. 4(c)],

because twelve is a multiple of six.

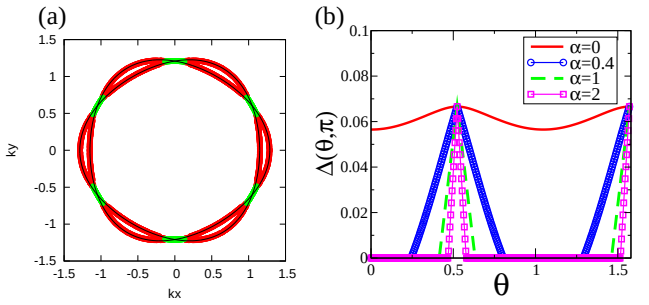

FIG. 5. (Color online) (a) A-FSs at the Brillouin zone face, $k_z = \pm\pi$. Gapless and gapped regions at $\alpha = 1$ are shown by red and green lines, respectively. (b) Angle dependence of the gap $\Delta(\theta, \pi)$ for various SOCs. The other parameters are the same as Fig. 3(b).

Now we show a gap node induced by the SOC. The nonsymmorphic space group allows a line node at the Brillouin zone face as pointed out by Norman[23] as a counterexample of Blount's theorem. Contrary to the Norman's argument, we obtain a *nodal arc* on the FSs. That is, a part of FS is gapped as shown in Fig. 5. Seemingly contradictory results are obtained because we plot the excitation gap near the FSs, $\Delta(\theta, \pi) = \mathrm{Min}_{k,n}|E_n(k\cos\theta, k\sin\theta, \pi)|$, although Norman's argument revealed the disappearance of intra-band Cooper pairs. The excitation spectrum is actually gapped around $\boldsymbol{k}_{\parallel} \parallel [010]$ owing to the inter-band Cooper pairing.

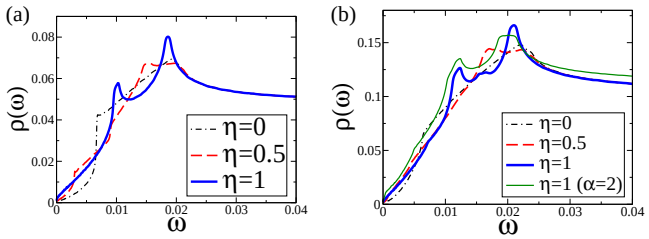

FIG. 6. (Color online) DOS of (a) a Γ-FS and (b) A-FSs. Parameters are the same as Fig. 3. We also show a result for $\alpha = 2$ in (b) by the thin green solid line in order to clarify the contribution of the SOC-induced arc node.

Finally, we show the DOS in Fig. 6. Even though the line node is absent in accordance with Blount's theorem, the DOS shows a linear energy dependence in the B-phase in agreement with experimental observations[11,12]. Although the SOC-induced arc node on the A-FSs[23] increases the DOS around $\omega = 0$, its contribution is not dominant, as shown in Fig. 6(b). Thus, it is indicated that at most 44 point nodes on paired A-FSs and 54 point nodes on three Γ-FSs give rise to line node-like behaviors. The thermal conductivity measurement has been a powerful tool in identifying the superconducting symmetry of UPt_3[12,19]. The saturating ratio κ_c/κ_b supporting the chiral f-wave state[12,53,54] also supports the generic E_{2u}-state which has point nodes on general points of Brillouin zone. A residual thermal conductivity much smaller than the universal value of line nodal superconductors[55] may be consistent with point nodal E_{2u}-state. Nearly isotropic ab-plane field-angle dependence[19,56] may be explained by the cancellation of anisotropy from nearly 100 point nodes.

A square-root dependence $\rho(\omega) \propto \sqrt{\omega}$ is obtained in the low-energy region at $\eta = 1$ [Fig. 6(a)] as a result of the quadratic line node. However, unusual $\sqrt{\omega}$-dependence may be obscured by the vortex scattering since $\eta = 1$ is not realized at zero magnetic field as illustrated in Fig. 1(a)[44].

Conclusion — To conclude, the E_{2u}-pairing-state in UPt_3 is a Weyl superconducting state of new type which shows the pair creation, pair annihilation, and coalescence of Weyl nodes. The p+d+f-mixing in the order parameter partly due to the nonsymmorphic crystal symmetry causes these unusual behaviors which have not been observed in a chiral f-wave state[35]. The topologically distinct properties give rise to Majorana arcs in surface states analogous to recently observed Fermi arc[28–30], resulting in a zero-field thermal Hall conductivity[34,35] and quasiparticle interference[57]. Tunable positions of Weyl nodes by temperature and magnetic field may enable experimental observations and also may induce the chiral anomaly through a topological defect in the combined real and momentum space[58].

Our results are compatible with Blount's theorem[20,21], but at most 98 point nodes and the SOC-induced arc node lead to line node behaviors in the DOS, consistent with experimental observations in UPt_3[12]. A generic E_{2u}-pairing-state studied here may also be consistent with experiments incompatible with the chiral f-wave state[13,19,55,56], although further theoretical developments taking account of multigap structure are desired.

Nonsymmorphic symmetry may be weakly broken either by a crystal distortion[59] or by an antiferromagnetic order in UPt_3[45,46]. Even in this case, the topologically protected Weyl nodes are robust, although the symmetry-protected SOC-induced arc node is gapped.

ACKNOWLEDGMENTS

The authors are grateful to K. Izawa, H. Harima, S. Kobayashi, T. Nomoto, M. Sato, and K. Shiozaki for fruitful discussions. This work was supported by the "Topological Quantum Phenomena" (No. JP25103711) and "J-Physics" (No. JP15H05884) Grant-in Aid for Scientific Research on Innovative Areas from MEXT of Japan, and by JSPS KAKENHI Grant Nos. JP24740230, JP15K05164, JP15H05745, and JP16H00991.

* yanase@scphys.kyoto-u.ac.jp

[1] C. L. Kane and E. J. Mele, Quantum Spin Hall Effect in Graphene, Phys. Rev. Lett. **95**, 226801 (2005).

[2] A. P. Schnyder, S. Ryu, A. Furusaki, and A. W. W. Ludwig, Classification of topological insulators and superconductors in three spatial dimensions, Phys. Rev. B **78**, 195125 (2008).

[3] A. Kitaev, Periodic table for topological insulators and superconductors, AIP Conf. Proc. No. 1134 (AIP, New York, 2009), p. 22.

[4] X.-L. Qi and S.-C. Zhang, Topological insulators and superconductors, Rev. Mod. Phys. **83**, 1057 (2011).

[5] Y. Yanase, T. Jujo, T. Nomura, H. Ikeda, T. Hotta and K. Yamada, Theory of superconductivity in strongly correlated electron systems, Phys. Rep. **387**, 1 (2003).

[6] G. R. Stewart, Z. Fisk, J. O. Willis, and J. L. Smith, Possibility of coexistence of bulk superconductivity and spin fluctuations in UPt_3, Phys. Rev. Lett. **52**, 679 (1984).

[7] R. A. Fisher, S. Kim, B. F. Woodfield, N. E. Phillips, L. Taillefer, K. Hasselbach, J. Flouquet, A. L. Giorgi, and J. L. Smith, Specific heat of UPt_3: Evidence for unconventional superconductivity, Phys. Rev. Lett. **62**, 1411 (1989).

[8] G. Bruls, D. Weber, B. Wolf, P. Thalmeier, B. Luthi, A. de Visser, and A. Menovsky, Strain-order-parameter coupling and phase diagrams in superconducting UPt_3, Phys. Rev. Lett. **65**, 2294 (1990).

[9] S. Adenwalla, S. W. Lin, Q. Z. Ran, Z. Zhao, J. B. Ketterson, J. A. Sauls, L. Taillefer, D. G. Hinks, M. Levy, and Bimal K. Sarma, Phase diagram of UPt_3 from ultrasonic velocity measurements, Phys. Rev. Lett. **65**, 2298 (1990).

[10] M. Sigrist and K. Ueda, Phenomenological theory of unconventional superconductivity, Rev. Mod. Phys. **63**, 239 (1991).

[11] J. A. Sauls, The order parameter for the superconducting phases of UPt_3, Adv. Phys. **43**, 113 (1994).

[12] R. Joynt and L. Taillefer, The superconducting phases of UPt_3, Rev. Mod. Phys. **74**, 235 (2002).

[13] H. Tou, Y. Kitaoka, K. Ishida, K. Asayama, N. Kimura, Y. Onuki, E. Yamamoto, Y. Haga, and K. Maezawa, Nonunitary spin-triplet superconductivity in UPt_3: evidence from ^{195}Pt Knight shift study, Phys. Rev. Lett. **80**, 3129 (1998).

[14] A. Y. Kitaev, Unpaired Majorana fermions in quantum wires, Phys. Usp. **44**, 131 (2001).

[15] M. Sato, Topological odd-parity superconductors, Phys. Rev. B **81**, 220504 (2010).

[16] Y. Tanaka, M. Sato, and N. Nagaosa, Symmetry and topology in superconductors -odd-frequency pairing and edge states-, J. Phys. Soc. Jpn. **81**, 011013 (2012).

[17] E. R. Schemm, W. J. Gannon, C. M. Wishne, W. P. Halperin, and A. Kapitulnik, Observation of broken time-reversal symmetry in the heavy-fermion superconductor UPt_3, Science **345**, 190 (2014).

[18] J. D. Strand, D. J. Bahr, D. J. Van Harlingen, J. P. Davis, W. J. Gannon, and W. P. Halperin, The transition between real and complex superconducting order parameter phases in UPt_3, Science **328**, 1368 (2010).

[19] Y. Machida, A. Itoh, Y. So, K. Izawa, Y. Haga, E. Yamamoto, N. Kimura, Y. Onuki, Y. Tsutsumi, and K. Machida, Twofold spontaneous symmetry breaking in the heavy-fermion superconductor UPt_3, Phys. Rev. Lett. **108**, 157002 (2012); K. Izawa, Y. Machida, A. Itoh, Y. So, K. Ota, Y. Haga, E. Yamamoto, N. Kimura, Y. Onuki, Y. Tsutsumi, and K. Machida, Pairing Symmetry of UPt3 Probed by Thermal Transport Tensors, J. Phys. Soc. Jpn. **83**, 061013 (2014).

[20] E. I. Blount, Symmetry properties of triplet superconductors, Phys. Rev. B **32**, 2935 (1985).

[21] S. Kobayashi, K. Shiozaki, Y. Tanaka, and M. Sato, Topological Blount's theorem of odd-parity superconductors, Phys. Rev. B **90**, 024516 (2014).

[22] A line node protected by a nonsymmorphic space group symmetry has been proposed[23] as a counterexample of Blount's theorem. Indeed, our model shows an arc node protected by the screw and glide symmetry of UPt_3. On the other hand, the line node in the chiral f-wave state is not protected by the nonsymmorphic symmetries.

[23] M. R. Norman, Odd parity and line nodes in heavy-fermion superconductors, Phys. Rev. B **52**, 15093 (1995); T. Micklitz and M. R. Norman, Odd parity and line nodes in nonsymmorphic superconductors, Phys. Rev. B **80**, 100506(R) (2009).

[24] T. Meng and L. Balents, Weyl superconductors, Phys. Rev. B **86**, 054504 (2012).

[25] S. Murakami, Phase transition between the quantum spin Hall and insulator phases in 3D: emergence of a topological gapless phase, New J. Phys. **9**, 356 (2007).

[26] X. Wan, A. M. Turner, A. Vishwanath, and S. Y. Savrasov, Topological semimetal and Fermi-arc surface states in the electronic structure of pyrochlore Iridates, Phys. Rev. B **83**, 205101 (2011).

[27] A. A. Burkov and L. Balents, Weyl semimetal in a topological insulator multilayer, Phys. Rev. Lett. **107**, 127205 (2011).

[28] S.-Y. Xu, I. Belopolski, N. Alidoust, M. Neupane, C. Zhang, R. Sankar, S.-M. Huang, C.-C. Lee, G. Chang, B. Wang, G. Bian, H. Zheng, D. S. Sanchez, F. Chou, H. Lin, S. Jia, and M. Z. Hasan, Discovery of a Weyl fermion semimetal and topological Fermi arcs, Science **349**, 613 (2015).

[29] B. Q. Lv, N. Xu, H. M. Weng, J. Z. Ma, P. Richard, X. C. Huang, L. X. Zhao, G. F. Chen, C. E. Matt, F. Bisti, V. N. Strocov, J. Mesot, Z. Fang, X. Dai, T. Qian, M. Shi, and H. Ding, Observation of Weyl nodes in TaAs, Nature Phys. **11**, 724 (2015).

[30] L. X. Yang, Z. K. Liu, Y. Sun, H. Peng, H. F. Yang, T. Zhang, B. Zhou, Y. Zhang, Y. F. Guo, M. Rahn, D. Prabhakaran, Z. Hussain, S.-K. Mo, C. Felser, B. Yan, and Y. L. Chen, Weyl semimetal phase in the non-centrosymmetric compound TaAs, Nature Phys. **11**, 728 (2015).

[31] X. Huang, L. Zhao, Y. Long, P. Wang, D. Chen, Z. Yang, H. Liang, M. Xue, H. Weng, Z. Fang, X. Dai, and G. Chen, Observation of the chiral-anomaly-induced negative magnetoresistance in 3D Weyl semimetal TaAs, Phys. Rev. X **5**, 031023 (2015).

[32] G. E. Volovik, Flat band in the core of topological defects: bulk-vortex correspondence in topological superfluids with Fermi points, JETP Lett. **93**, 66 (2011).

[33] J. D. Sau and S. Tewari, Topologically protected surface Majorana arcs and bulk Weyl fermions in ferromagnetic superconductors, Phys. Rev. B **86**, 104509 (2012).

[34] M. H. Fischer, T. Neupert, C. Platt, A. P. Schnyder, W. Hanke, J. Goryo, R. Thomale, and M. Sigrist, Chi-

ral d-wave superconductivity in SrPtAs, Phys. Rev. B **89**, 020509 (2014).
[35] P. Goswami and A. H. Nevidomskyy, Topological Weyl superconductor to diffusive thermal Hall metal crossover in the B phase of UPt_3, Phys. Rev. B **92**, 214504 (2015).
[36] Y. Saito, Y. Nakamura, M. S. Bahramy, Y. Kohama, J. Ye, Y. Kasahara, Y. Nakagawa, M. Onga, M. Tokunaga, T. Nojima, Y. Yanase, Y. Iwasa, Superconductivity protected by spin-valley locking in gate-tuned MoS_2, Nat. Phys. **12**, 144 (2016).
[37] M. H. Fischer, F. Loder, and M. Sigrist, Superconductivity and local noncentrosymmetricity in crystal lattices, Phys. Rev. B **84**, 184533 (2011).
[38] D. Maruyama, M. Sigrist, and Y. Yanase, Locally noncentrosymmetric superconductivity in multilayer systems, J. Phys. Soc. Jpn. **81**, 034702 (2012).
[39] L. Taillefer and G. G. Lonzarich, Heavy-fermion quasiparticles in UPt_3, Phys. Rev. Lett. **60**, 1570 (1988); M. R. Norman, R. C. Albers, A. M. Boring, and N. E. Christensen, Fermi surface and effective masses for the heavy-electron superconductors UPt_3, Solid State Commun. **68**, 245 (1988).
[40] N. Kimura, R. Settai, Y. Onuki, H. Toshima, E. Yamamoto, K. Maezawa, H. Aoki, and H. Harima, Magnetoresistance and de Haas-van Alphen effect in UPt_3, J. Phys. Soc. Jpn. **64**, 3881 (1995).
[41] G. J. McMullan, P. M. C. Rourke, M. R. Norman, A. D. Huxley, N. Doiron-Leyraud, J. Flouquet, G. G. Lonzarich, A. McCollam, and S. R. Julian, The Fermi surface and f-valence electron count of UPt_3, New J. Phys, **10**, 053029 (2008).
[42] T. Nomoto and H. Ikeda, Exotic multi-gap structure in UPt_3 unveiled by the first-priniciples analysis, arXiv:1607.02708.
[43] See Appendix A for a theoretical derivation of order parameter in a generic E_{2u} state.
[44] The range of the parameter η is listed in Appendix C (Table. II). The temperature and magnetic field dependence of the parameter η is explained in details on the basis of the Ginzburg-Landau theory.
[45] G. Aeppli, E. Bucher, C. Broholm, J. K. Kjems, J. Baumann and J. Hufnagl, Magnetic order and fluctuations in superconducting UPt_3, Phys. Rev. Lett. **60**, 615 (1988).
[46] S. M. Hayden, L. Taillefer, C. Vettier, and J. Flouquet, Antiferromagnetic order in UPt_3 under pressure: evidence for a direct coupling to superconductivity, Phys. Rev. B **46**, 8675(R) (1992).
[47] D. J. Thouless, M. Kohmoto, M. P. Nightingale, and M. den Nijs, Quantized Hall conductance in a two-dimensional periodic potential, Phys. Rev. Lett. **49**, 405 (1982).
[48] M. Kohmoto, Topological invariant and the quantization of the Hall conductance, Ann. Phys. **160**, 343 (1985).
[49] T. Fukui, Y. Hatsugai, and H. Suzuki, Chern numbers in discretized Brillouin zone: efficient method of computing (spin) Hall conductances, J. Phys. Soc. Jpn. **74**, 1674 (2005).
[50] Analytic results of nodal structure in the single band model are shown in Appendix B.
[51] In the presence of the time-reversal symmetry, the BdG Hamiltonian on a generic two-dimensional momentum space belongs to the symmetry class AIII[2,3]. Then, the Chern number on a closed surface must be zero.
[52] The degeneracy of two bands at $k_z = \pi$ and $\boldsymbol{k}_{\parallel} \parallel [010]$ (A-L lines) is protected by the crystal symmetry. This is proved by using the relations, $\{IG_{xz}, IT\} = 0$, $\{IG_{xz}, M_{yz}\} = 0$, and $(IG_{xz})^2 = -1$, at $k_z = \pm\pi$. Inversion symmetry, time-reversal symmetry, and mirror symmetry are represented by $I = \sigma_x$, $T = is_yK$, and $M_{yz} = is_x$, respectively. The glide symmetry is represented by $G_{xz} = s_y\sigma_y$ at $k_z = \pm\pi$ while $G_{xz} = is_y\sigma_x$ at $k_z = 0$. We will show details elsewhere.
[53] B. Lussier, B. Ellman, and L. Taillefer, Determination of the gap structure in UPt_3 by thermal conductivity, Phys. Rev. B **53**, 5145 (1996).
[54] M. R. Norman and P. J. Hirschfeld, Heat transport and the nature of the order parameter in superconducting UPt_3, Phys. Rev. B **53**, 5706 (1996).
[55] H. Suderow, J. P. Brison, A. D. Huxley, and J. Flouquet, Thermal conductivity and gap structure of the superconducting phases of UPt_3, J. Low Temp. Phys. **108**, 11 (1997).
[56] S. Kittaka, K. An, T. Sakakibara, Y. Haga, E. Yamamoto, N. Kimura, Y. Onuki, and K. Machida, Anomalous Field-Angle Dependence of the Specific Heat of Heavy-Fermion Superconductor UPt_3, J. Phys. Soc. Jpn. **82**, 024707 (2013).
[57] S. Kourtis, J. Li, Z. Wang, A. Yazdani, and B. A. Bernevig, Universal signatures of Fermi arcs in quasiparticle interference on the surface of Weyl semimetals, Phys. Rev. B **93**, 041109(R) (2016).
[58] G. E. Volovik, Topology of chiral superfluid: skyrmions, Weyl fermions and chiral anomaly, JETP Lett. **103**, 140 (2016).
[59] D. A. Walko, J.-I. Hong, T. V. Chandrasekhar Rao, Z. Wawrzak, D. N. Seidman, W. P. Halperin, and M. J. Bedzyk, Crystal structure assignment for the heavy-fermion superconductor UPt_3, Phys. Rev. B **63**, 054522 (2001).

Appendix A: Order Parameter in E_{2u} Representation of D_{6h} Point Group with Nonsymmorphic Operation

In the presence of spin-orbit coupling, superconducting states are classified by crystal point group symmetry. The order parameter should belong to an irreducible representation of the point group[10]. In this paper we adopt the order parameter of superconductivity in the E_{2u} representation of D_{6h} point group symmetry. List of characters of the two-dimensional E_{2u} representation is shown in Table I. Basis functions are composed of the p-wave component, $\left(\hat{\Gamma}_1, \hat{\Gamma}_2\right) = (p_x\hat{x} - p_y\hat{y}, p_y\hat{x} + p_x\hat{y})$, and the f-wave component, $\left(f_{(x^2-y^2)z}\hat{z}, f_{xyz}\hat{z}\right)$, in the absence of the orbital and sublattice degrees of freedom[12].

On the other hand, the crystal structure of UPt_3 is composed of two sublattices at $z = 0$ and $z = 1/2$. The local symmetry of Uranium ions is D_{3h} which lacks inversion symmetry, while the stacking of Uranium ions along the c axis recovers the inversion symmetry and ensures the point group D_{6h}. In this crystal structure, a half of symmetry operations of the D_{6h} point group, which are not included in the D_{3h} point group, is accompanied by a half translation along the c axis. For instance, glide symmetry $\{\sigma_v|\frac{\hat{c}}{2}\}$ and screw symmetry $\{C_6|\frac{\hat{c}}{2}\}$ are preserved instead of σ_v mirror symmetry and C_6 rotation symmetry. Thus, the space group is nonsymmorphic. Then, we can show that the sublattice-singlet spin-triplet d-wave component, $\left(\hat{\Gamma}_1, \hat{\Gamma}_2\right) = (d_{yz}\hat{z}, d_{xz}\hat{z})\,\sigma_y$, is also a basis function of the E_{2u} representation. Indeed, the symmetry operations on the d-wave component are specified by the characters of the E_{2u} representation as we show in Table I, although the conventional (sublattice-triplet spin-singlet) d-wave state belongs to the E_{1g} representation.

	E	$2C_3$	$3C_2'$	$2S_3$	σ_h	$3\sigma_d$	$2\{C_6\|\frac{c}{2}\}$	$\{C_2\|\frac{c}{2}\}$	$3C_2''$	I	S_6	$3\{\sigma_v\|\frac{c}{2}\}$	Basis function
E_{2u}	2	-1	0	1	-2	0	-1	2	0	-2	1	0	$(k_x\hat{x} - k_y\hat{y}, k_y\hat{x} + k_x\hat{y})$, $(k_x^2 - k_y^2, 2k_xk_y)k_z\hat{z}$, $(k_yk_z, k_zk_x)\hat{z}\sigma_y$
E_{1g}	2	-1	0	1	-2	0	1	-2	0	2	-1	0	(k_zk_x, k_yk_z)

TABLE I. List of characters for the E_{2u} and E_{1g} representations of the D_{6h} point group. The last column shows basis functions.

One may suppose that the sublattice-singlet spin-triplet d-wave component requires an exotic Cooper pairing. However, it naturally appears when we adopt short-range Cooper pairs. We take into account the nearest-neighboring Cooper pairs formed on the $\boldsymbol{r}_i$-bonds, that is shown in Fig. 1(b). The pairing field by each bond is obtained as, $\Delta_i \sin\frac{k_z}{2} e^{i\boldsymbol{k}_\parallel\cdot\boldsymbol{r}_i}$, with $i = 1, 2, 3$. The order parameter compatible with E_{2u} irreducible representation is given by

$$\hat{\Delta}_{d+f}(\boldsymbol{k}) = \begin{pmatrix} 0 & \sum_i \Delta_i \sin\frac{k_z}{2} e^{i\boldsymbol{k}_\parallel\cdot\boldsymbol{r}_i} \\ \sum_i \Delta_i \sin\frac{k_z}{2} e^{-i\boldsymbol{k}_\parallel\cdot\boldsymbol{r}_i} & 0 \end{pmatrix}_\sigma \otimes is_zs_y. \tag{A1}$$

The real part proportional to σ_x may have f-wave symmetry. Taking appropriate linear combination, we obtain the orbital functions of f_{xyz}-wave and $f_{(x^2-y^2)z}$-wave components,

$$f_{xyz}(\boldsymbol{k}) = -\sqrt{3}\sin\frac{k_z}{2}\mathrm{Re}\sum_i r_i^x e^{i\boldsymbol{k}_\parallel\cdot\boldsymbol{r}_i}, \tag{A2}$$

$$f_{(x^2-y^2)z}(\boldsymbol{k}) = -\sqrt{3}\sin\frac{k_z}{2}\mathrm{Re}\sum_i r_i^y e^{i\boldsymbol{k}_\parallel\cdot\boldsymbol{r}_i}. \tag{A3}$$

The imaginary part of Eq. (A1) is represented by the Pauli matrix σ_y and the symmetry is d-wave. The same linear combination as Eqs. (A2) and (A3) gives the orbital functions of d_{xz}-wave and d_{yz}-wave components,

$$d_{xz}(\boldsymbol{k}) = -\sqrt{3}\sin\frac{k_z}{2}\mathrm{Im}\sum_i r_i^x e^{i\boldsymbol{k}_\parallel\cdot\boldsymbol{r}_i}, \tag{A4}$$

$$d_{yz}(\boldsymbol{k}) = -\sqrt{3}\sin\frac{k_z}{2}\mathrm{Im}\sum_i r_i^y e^{i\boldsymbol{k}_\parallel\cdot\boldsymbol{r}_i}. \tag{A5}$$

By using these orbital functions, the order parameter of Cooper pairs on the $\boldsymbol{r}_i$-bonds is written as

$$\hat{\Delta}_{d+f}(\boldsymbol{k}) = \eta_1\left[f_{(x^2-y^2)z}(\boldsymbol{k})\sigma_x - d_{yz}(\boldsymbol{k})\sigma_y\right]s_zis_y + \eta_2\left[f_{xyz}(\boldsymbol{k})\sigma_x - d_{xz}(\boldsymbol{k})\sigma_y\right]s_zis_y. \tag{A6}$$

Thus, the d-wave component naturally accompanies with the f-wave component as a result of the crystal structure of UPt_3. In other words, the Cooper pairs on the $\boldsymbol{r}_i$-bonds give rise to superconducting order parameters having composite d+f-wave momentum dependence. Equation (A6) is a part of Eqs. (2) and (3) in the main text.

Because the p-wave component also belongs to the E_{2u} irreducible representation, it naturally coexists with the above $d+f$-wave component owing to the spin-orbit coupling. In this paper we adopt p-wave Cooper pairs formed on the intra-layer nearest-neighboring $\boldsymbol{e}_i$-bonds. Then, the order parameter compatible with E_{2u} irreducible representation is

$$\hat{\Delta}_p(\boldsymbol{k}) = \eta_1\big[p_x(\boldsymbol{k})s_x - p_y(\boldsymbol{k})s_y\big]\sigma_0 i s_y + \eta_2\big[p_y(\boldsymbol{k})s_x + p_x(\boldsymbol{k})s_y\big]\sigma_0 i s_y, \tag{A7}$$

and the orbital functions are given by

$$p_x(\boldsymbol{k}) = \sum_i e_i^x \sin \boldsymbol{k}_\parallel \cdot \boldsymbol{e}_i, \tag{A8}$$

$$p_y(\boldsymbol{k}) = \sum_i e_i^y \sin \boldsymbol{k}_\parallel \cdot \boldsymbol{e}_i. \tag{A9}$$

Taking into account the mixing of the $d+f$-wave Cooper pairs on the $\boldsymbol{r}_i$-bonds and the p-wave Cooper pairs on the $\boldsymbol{e}_i$-bonds, we adopt a linear combination $\hat{\Delta}(\boldsymbol{k}) = \delta\hat{\Delta}_p(\boldsymbol{k}) + \hat{\Delta}_{d+f}(\boldsymbol{k})$. Then, the basis functions of generic E_{2u} state are given by Eqs. (2) and (3) in the main text. To be compatible with experiments, we assume that the weight of p-wave component is small, $|\delta| \ll 1$.

Recently, the mixing of p-wave, d-wave, and f-wave order parameters was demonstrated by a microscopic theory based on first principle band structure calculation[42]. Although the weight of p-, d-, and f-wave components obtained in Ref.[42] is unlikely to be compatible with experiments[12], it is indicated that mixing of order parameters naturally occurs owing to the many body effect. Generally speaking, symmetry-allowed interactions effectively appear in solid state electron systems through the many body effect. Therefore, symmetry-allowed mixing in order parameter naturally occurs.

It should be noticed that the inter-sublattice $d+f$-wave Cooper pairs and the intra-sublattice p-wave ones are taken into account. Intra-sublattice f-wave Cooper pairs as well as inter-sublattice p-wave ones may also be induced by a longer-range pairing. However, we have confirmed that those components do not alter our results as far as the $d+f$-wave component is a dominant order parameter.

Note that the short-range Cooper pairs have been identified in many unconventional superconductors by microscopic theories for the strongly correlated electron systems[5]. Thus, the order parameter derived above is a reasonable assumption. Although it is desirable to calculate the order parameter with the use of microscopic theories, satisfactory theory has not been developed for Uranium-based heavy fermion superconductors up to now.

Appendix B: Nodal structure in a single band model

Any single band model does not reproduce the nodal structure on the paired A-FSs illustrated in Figs. 4 and 5, because the nonsymmorphic crystal symmetry and associated multiband structure are not taken into account. On the other hand, the Weyl node, quadratic line node, and cubic point node on the Γ-FS (Fig. 2) are obtained even in the single band model. These unusual nodal structures are indeed induced by the p-f-mixing in the order parameter, and then the multiband structure and spin-orbit coupling do not play any role. Analytic results of nodal structures are obtained in the single band model, which we show below for a transparent understanding of Fig. 2.

We consider the basis function composed of the p-wave and f-wave components,

$$\hat{\Gamma}_1 = \big[\delta\left\{p_x(\boldsymbol{k})s_x - p_y(\boldsymbol{k})s_y\right\} + f_{(x^2-y^2)z}(\boldsymbol{k})s_z\big] i s_y, \tag{B1}$$

$$\hat{\Gamma}_2 = \big[\delta\left\{p_y(\boldsymbol{k})s_x + p_x(\boldsymbol{k})s_y\right\} + f_{xyz}(\boldsymbol{k})s_z\big] i s_y. \tag{B2}$$

The order parameter in the chiral superconducting state, $\hat{\Delta}(\boldsymbol{k}) = \Delta_0\left(\hat{\Gamma}_1 + i\eta\hat{\Gamma}_2\right)$, is described by the d-vector

$$\boldsymbol{d}(\boldsymbol{k}) = \Delta_0\left[\delta\left\{p_x(\boldsymbol{k})\hat{x} - p_y(\boldsymbol{k})\hat{y}\right\} + i\eta\delta\left\{p_y(\boldsymbol{k})\hat{x} + p_x(\boldsymbol{k})\hat{y}\right\} + f_{(x^2-y^2)z}(\boldsymbol{k})\hat{z} + i\eta f_{xyz}(\boldsymbol{k})\hat{z}\right]. \tag{B3}$$

Because the order parameter is non-unitary[10], the superconducting gap $\Delta_\pm(\boldsymbol{k})$ is obtained by

$$\Delta_\pm(\boldsymbol{k})^2 = |\boldsymbol{d}(\boldsymbol{k})|^2 \pm |i\boldsymbol{d}(\boldsymbol{k}) \times \boldsymbol{d}(\boldsymbol{k})^*|^2 \tag{B4}$$

$$= \Delta_0^2\left[\left(1+\eta^2\right)|p(\boldsymbol{k})|^2 + |f_{(x^2-y^2)z}(\boldsymbol{k})|^2 + \eta^2|f_{xyz}(\boldsymbol{k})|^2 \pm 2\sqrt{\eta^2|p(\boldsymbol{k})|^2\left(|p(\boldsymbol{k})|^2 + |f(\boldsymbol{k})|^2\right)}\right], \tag{B5}$$

with $|p(\boldsymbol{k})|^2 = \delta^2\left(|p_x(\boldsymbol{k})|^2 + |p_y(\boldsymbol{k})|^2\right)$ and $|f(\boldsymbol{k})|^2 = \left(|f_{(x^2-y^2)z}(\boldsymbol{k})|^2 + |f_{xyz}(\boldsymbol{k})|^2\right)$. For $\eta \leq 1$, the condition for a nodal gap, $\Delta_-(\boldsymbol{k}) = 0$, is satisfied when

$$f_{(x^2-y^2)z}(\boldsymbol{k}) = 0 \quad \text{and} \quad \left(1-\eta^2\right)|p(\boldsymbol{k})|^2 = \eta^2 |f_{xyz}(\boldsymbol{k})|^2. \tag{B6}$$

On the other hand, for $\eta \geq 1$ the small gap $\Delta_-(\boldsymbol{k})$ may have nodes at $\boldsymbol{k}$ with

$$f_{xyz}(\boldsymbol{k}) = 0 \quad \text{and} \quad \left(\eta^2-1\right)|p(\boldsymbol{k})|^2 = |f_{(x^2-y^2)z}(\boldsymbol{k})|^2. \tag{B7}$$

Hence, the nodal structure is clarified by solving Eqs. (B6) and (B7).

Let us assume an isotropic Fermi surface at $\boldsymbol{k} = k_{\rm F}(\sin\theta\cos\phi, \sin\theta\sin\phi, \cos\theta)$ for simplicity. Then, we naturally adopt the long wave length approximation,

$$[p_x(\boldsymbol{k}), p_y(\boldsymbol{k})] = (k_x, k_y)/k_{\rm F} = k\sin\theta(\cos\phi, \sin\phi)/k_{\rm F}, \tag{B8}$$

$$\left[f_{(x^2-y^2)z}(\boldsymbol{k}), f_{xyz}(\boldsymbol{k})\right] = (k_x^2 - k_y^2, 2k_xk_y)k_z/k_{\rm F}^3 = k^3\sin^2\theta\cos\theta(\cos 2\phi, \sin 2\phi)/k_{\rm F}^3. \tag{B9}$$

Solving Eq. (B6), we find point nodes at $\phi = n\pi/2 + \pi/4$ with n being an integer and

$$\theta = \pi/4 \pm \left[\pi/4 - \frac{1}{2}\arcsin\left(2\delta\sqrt{\eta^{-2}-1}\right)\right], 3\pi/4 \pm \left[\pi/4 - \frac{1}{2}\arcsin\left(2\delta\sqrt{\eta^{-2}-1}\right)\right]. \tag{B10}$$

Equation (B7) is satisfied at the momentum, $\phi = n\pi/2$ and

$$\theta = \pi/4 \pm \left[\pi/4 - \frac{1}{2}\arcsin\left(2\delta\sqrt{\eta^{2}-1}\right)\right], 3\pi/4 \pm \left[\pi/4 - \frac{1}{2}\arcsin\left(2\delta\sqrt{\eta^{2}-1}\right)\right]. \tag{B11}$$

From these results we find that the pair creation of Weyl nodes occurs at momentum $\boldsymbol{k} = k_{\rm F}\left(\pm\frac{1}{2}, \pm\frac{1}{2}, \pm\frac{1}{\sqrt{2}}\right)$ when $\eta = \eta_{\rm c} \equiv \left(1 + 1/4\delta^2\right)^{-1/2}$ while at $\boldsymbol{k} = k_{\rm F}\left(\pm\frac{1}{\sqrt{2}}, 0, \pm\frac{1}{\sqrt{2}}\right)$ and $k_{\rm F}\left(0, \pm\frac{1}{\sqrt{2}}, \pm\frac{1}{\sqrt{2}}\right)$ when $\eta = \eta_{\rm c}^{-1}$. Thus, the superconducting state hosts eight pairs of Weyl nodes for $\eta_{\rm c} < \eta < \eta_{\rm c}^{-1}$. These features of Weyl nodes have been demonstrated in the two-band model reproducing the Γ-FS (Fig. 2 in the main text). Trivial point nodes are present at $\theta = 0$ and π independent of the parameter η, since $p_x(\boldsymbol{k}) = p_y(\boldsymbol{k}) = f_{(x^2-y^2)z}(\boldsymbol{k}) = f_{xyz}(\boldsymbol{k}) = 0$ at $\boldsymbol{k}_\parallel = 0$.

At $\eta = 1$, Eqs. (B6) and (B7) are satisfied at $k_z = 0$, leading to the quadratic line node at the equator of Fermi surface. Then, the positions of Weyl nodes discussed above are reduced to $\theta = 0$, $\pi/2$, and π, indicating the pair annihilation at the equator of Fermi surface and the coalescence at the poles. Considering rotation symmetry, we understand the pair annihilation and coalescence of Weyl nodes. Six-fold rotation symmetry is preserved at and only at $\eta = 1$. Then, the number of Weyl nodes at $\boldsymbol{k}_\parallel \neq 0$ (defined as W') has to be a multiple of six. Since $W' = 16$ at $\eta \neq 1$, it must change at $\eta = 1$. It actually changes to $W' = 0$ as a result of the pair annihilation and coalescence of Weyl nodes.

At $\eta = 1$, the quadratic line node at $k_z = 0$ and the cubic point nodes at $\boldsymbol{k}_\parallel = 0$ are obtained from Eq. (B5). Because the f-wave component vanishes at these momentum, we can approximate the superconducting gap around the nodal region,

$$\Delta_-(\boldsymbol{k})^2 = \Delta_0^2\left[2|p(\boldsymbol{k})|^2 + |f(\boldsymbol{k})|^2 - 2\sqrt{|p(\boldsymbol{k})|^2\left(|p(\boldsymbol{k})|^2 + |f(\boldsymbol{k})|^2\right)}\right] \simeq \Delta_0^2\frac{|f(\boldsymbol{k})|^4}{4|p(\boldsymbol{k})|^2}, \tag{B12}$$

$$\propto k_z^4 \qquad \text{around} \;\; k_z = 0, \tag{B13}$$

$$\propto |\boldsymbol{k}_\parallel|^6 \quad \text{around} \;\; \boldsymbol{k}_\parallel = 0. \tag{B14}$$

Equation (B13) shows the quadratic line node, $\Delta_-(\boldsymbol{k}) \propto k_z^2$, at the equator, while Eq. (B14) shows the cubic point node, $\Delta_-(\boldsymbol{k}) \propto |\boldsymbol{k}_\parallel|^3$, at the poles. These higher-order nodal structures are also obtained in the two-band model (see the discussion in the main text). From Eq. (B5) we also obtain the linear point node in the high-energy branch, $\Delta_+(\boldsymbol{k}) \propto |\boldsymbol{k}_\parallel|$, at $\boldsymbol{k}_\parallel = 0$.

In the next section S3, we show that the superconducting state with $\eta = 1$ is not realized at zero magnetic field on the basis of the Ginzburg-Landau theory. Although the magnetic field may realize $\eta = 1$ through the symmetry breaking term, the unusual nodal structures may be obscured in the vortex state.

Appendix C: Ginzburg-Landau Theory and Range of Parameter η

The order parameter of superconductivity in the E_{2u} representation is formally represented by

$$\hat{\Delta}(\boldsymbol{k}) = \eta_1\hat{\Gamma}_1 + \eta_2\hat{\Gamma}_2, \tag{C1}$$

and the basis functions $\hat{\Gamma}_1$ and $\hat{\Gamma}_2$ are shown in Sec. S1. The two component order parameters η_1 and η_2 are parametrized by

$$(\eta_1, \eta_2) = \Delta(1, i\eta)/\sqrt{1+\eta^2}. \tag{C2}$$

The ratio η characterizes internal structure of Cooper pairs, which depends on temperature and magnetic field. Previous studies on UPt_3 revealed the range of η listed in Table II[11,12]. The η in the A- and C-phases may be $(\eta_A, \eta_C) = (0, \infty)$ or $(\eta_A, \eta_C) = (\infty, 0)$. We assume the latter without loss of generality. Then, the η changes from 0 to ∞ in the B-phase, while it is zero (infinite) in the C-phase (A-phase).

A-phase	$\eta = \infty$
B-phase	$0 \le \eta \le \infty$
C-phase	$\eta = 0$

TABLE II. Range of the parameter η in the A-, B-, and C-phases of UPt_3[11,12].

Below we prove the list in Table II on the basis of the Ginzburg-Landau theory. Since the A-B transition and B-C transition in the superconducting state are second order phase transition[11,12], it is satisfactory to show the parameter η in the A- and C-phases. The parameter η must change continuously through the second order phase transitions, and therefore, it changes from ∞ to 0 along the line in Fig. 7 drawing the H-T phase diagram. We also show that a special condition $\eta = 1$ is not realized at zero magnetic field.

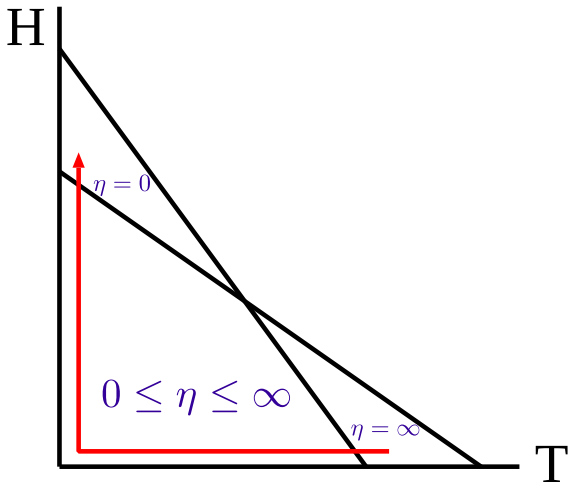

FIG. 7. (Color online) Illustration of the magnetic field-temperature phase diagram of UPt_3[12]. The parameter η in the A-, B-, and C-phases is shown. The A-phase with $\eta = \infty$ is stabilized by a symmetry breaking term F_1 which may be induced by a weak antiferromagnetic order. The C-phase with $\eta = 0$ is stabilized by another symmetry breaking term $F_1^{\rm grad}$ which renormalizes the coherence length. Because the A-B transition and B-C transition are second order phase transition and any first order transition does not occur in the B-phase, the parameter η has to change from ∞ to 0 when we move along the red arrow.

The Ginzburg-Landau free energy density for chiral superconductors is given by $F_0 + F_0^{\rm grad}$ with

$$F_0 = \alpha(|\eta_1|^2 + |\eta_2|^2) + \frac{\beta_1}{2}(|\eta_1|^2 + |\eta_2|^2)^2 + \frac{\beta_2}{2}(\eta_1\eta_2^* - \text{c.c.})^2 + \beta_3|\eta_1|^2|\eta_2|^2, \tag{C3}$$

$$\begin{aligned} F_0^{\rm grad} = {} & \kappa_1(|D_{\rm x}\eta_1|^2 + |D_{\rm y}\eta_2|^2) + \kappa_2(|D_{\rm x}\eta_2|^2 + |D_{\rm y}\eta_1|^2) + \kappa_5(|D_{\rm z}\eta_1|^2 + |D_{\rm z}\eta_2|^2) \\ & + \kappa_3\big[(D_{\rm x}\eta_1)(D_{\rm y}\eta_2)^* + \text{c.c.}\big] + \kappa_4\big[(D_{\rm x}\eta_2)(D_{\rm y}\eta_1)^* + \text{c.c.}\big], \end{aligned} \tag{C4}$$

for the two-component order parameters (η_1, η_2) in the two-dimensional irreducible representation[10–12], where $\alpha = \alpha_0\left(\frac{T}{T_{\rm c0}} - 1\right)$ and $D_j = -i\partial_j + (2\pi/\Phi_0)A_j$ are covariant derivatives. The hexagonal $D_{6\rm h}$ point group symmetry imposes relations, $\beta_3 = 0$ and $\kappa_3 = \kappa_4 = (\kappa_1 - \kappa_2)/2$.

We can drop the gradient term at zero magnetic field and obtain the order parameters by minimizing the homogeneous term F_0. The superconducting state is determined by the sign of β_2. The chiral state, $(\eta_1, \eta_2) = \Delta_0(\pm i, 1)$,

is stable for $\beta_2 > 0$, while a non-chiral state, $(\eta_1, \eta_2) = \Delta_0(\cos\theta, \sin\theta)$, is stable for $\beta_2 < 0$. The weak coupling BCS theory results in $\beta_2/\beta_1 = 1/3$, and experimental results in UPt_3 are fitted by $\beta_2/\beta_1 = 0.16 \sim 0.33$[11]. Thus, we assume $\beta_2 > 0$.

It is believed that the six-fold rotation symmetry is weakly broken in UPt_3[11] possibly by the antiferromagnetic order[45,46]. The symmetry breaking field yields a quadratic term,

$$F_1 = \alpha_0\epsilon_0 \left(|\eta_1|^2 - |\eta_2|^2\right), \tag{C5}$$

and splits the transition temperature of the Γ_1-state and the Γ_2-state. Here $\epsilon_0 > 0$ is assumed without loss of generality. By minimizing $F_0 + F_1$, we obtain the transition temperature of the A-phase, $T_c^A = (1+\epsilon_0)\, T_{c0}$, and the A-B transition temperature, $T_c^B = T_c^A - \frac{\beta_1}{\beta_2}\epsilon_0 T_{c0}$. The order parameter in the A-phase is obtained as $\eta_1 = 0$ and

$$\eta_2 = \sqrt{\frac{\alpha_0}{\beta_1 T_{c0}}\,(T_c^A - T)}. \tag{C6}$$

Thus, the parameter $\eta = \infty$ is consistent with the list in Table II.

In the B-phase, $(\eta_1, \eta_2) = (\pm i|\eta_1|, |\eta_2|)$ and

$$\begin{pmatrix} |\eta_1|^2 \\ |\eta_2|^2 \end{pmatrix} = -\begin{pmatrix} \beta_1 & \beta_1 - 2\beta_2 \\ \beta_1 - 2\beta_2 & \beta_1 \end{pmatrix}^{-1} \begin{pmatrix} \alpha_- \\ \alpha_+ \end{pmatrix}, \tag{C7}$$

where $\alpha_\pm = \alpha_0 \left(\frac{T}{T_{c0}} - 1 \mp \epsilon_0\right)$. Thus, we obtain the parameter η characterizing the chiral superconducting state,

$$\eta = \sqrt{\frac{\beta_1\alpha_+ - (\beta_1 - 2\beta_2)\alpha_-}{\beta_1\alpha_- - (\beta_1 - 2\beta_2)\alpha_+}}. \tag{C8}$$

Because $\alpha_\pm < 0$ and $|\alpha_-| < |\alpha_+|$, we obtain $\eta > 1$ in the whole B-phase at $H = 0$. When the temperature is decreased from T_c^B, the ratio of two-component order parameters changes from $\eta(T = T_c^B) = \infty$ to $\eta(T = 0) > 1$. Thus, the superconducting state hosting unusual quadratic line node at $k_z = 0$ is not realized at zero magnetic field.

Now we turn to the superconducting state in the magnetic field. When the anisotropy in the Fermi surface is neglected, the mean field theory for the f-wave state gives a rather simple relations in the gradient term, $\kappa_3 = \kappa_4 = 0$ and $\kappa_1 = \kappa_2$. Then, the gradient term is simplified as,

$$F_0^{\rm grad} = \kappa_1 \left(|\vec{D}\eta_1|^2 + |\vec{D}\eta_2|^2\right) + \kappa_5 \left(|D_z\eta_1|^2 + |D_z\eta_2|^2\right), \tag{C9}$$

with using $\vec{D} = (D_x, D_y)$. The symmetry breaking field gives rise to a correction to the gradient term

$$F_1^{\rm grad} = \epsilon_\parallel \left(|\vec{D}\eta_1|^2 - |\vec{D}\eta_2|^2\right) + \epsilon_\perp \left(|D_z\eta_1|^2 - |D_z\eta_2|^2\right). \tag{C10}$$

The parameters are chosen as $\epsilon_\parallel < 0$ and $\epsilon_\perp < 0$ so as to reproduce the multiple phase diagram in UPt_3[11]. Then, the orbital effect favors the Γ_1-state having a short coherence length. Thus, the $F_1^{\rm grad}$ term competes with the F_1 term. Since the former is more important than the latter at high magnetic fields, the Γ_1-state is stabilized in the high magnetic field C-phase. Thus, we obtain the parameter $\eta = 0$ in the C-phase consistent with the list in Table II. In the B-phase, the parameter η is decreased through $\eta = 1$ with increasing the magnetic field, and reaches to $\eta = 0$ at the B-C-phase boundary. This scenario proposed by Sauls[11] is consistent with the multiple superconducting phases in UPt_3 and has been regarded as the most promising scenario[12]. We also adopt this scenario and assume the range of the parameter η listed in Table II.